New technique to enhance the accuracy of 2-D/3-D field quantities and forces obtained by standard finite-element solutions

K.Hameyer
R.Mertens
U.Pahner
R.Belmans

Indexing terms: Electromagnetic energy transducers, Laplace equation, Fourier series, Dirichlet problem, Finite-element test models

Abstract: Useful energy conversion in electromagnetic energy transducers takes place only in the air gap. Numerical field computation techniques which have a range of general applications are used for the design and optimisation of these electromagnetic devices. To predict their operational behaviour, particular attention has to be paid to the computation of the air gap values of the flux densities and the magnetic field strength. Ongoing research on force computations in electromagnetic devices using different approaches indicates the importance of this field. A new method for the accurate computation of the field quantities and, thus, the generated forces in two- and three-dimensional finite-element models, is presented. Solving a local Dirichlet problem analytically enhances the accuracy of the derived field quantities using a numerically computed potential solution. Derivatives required for the values of the flux density are calculated analytically, in order to improve their order of convergence towards the exact solution. A Fourier series is used to represent the local field solution of two- and three-dimensional problems. The paper is focused on the practical application of the static electromagnetic field solution of the Laplace equation in a local post-process. Finite-element test models using standard first-order elements are applied to demonstrate the proposed method. Advantages and drawbacks are discussed.

1 Introduction

To predict the forces that are the key to the behaviour of several classes of electromagnetic devices, the solution requires the highest possible accuracy. Force and field quantities are derivatives of a potential formulation. The difficulty is owing to the fact that the FEM piecewise approximates the real potential by simple shape functions, instead of obtaining the exact solution [1]. Accounting for this, and assuming a small value of h as the maximum characteristic diameter of a finite element, the FEM is convergent towards the exact solution of order $q + 1$. The constant q describes the polynomial order of the elements used. With ε as the global error, the order of convergence for the potential solution is

$$\|\varepsilon\| \leq C \cdot h^{q+1} \tag{1}$$

The factor C is independent of the size h of the elements and depends only on the type of discretisation, choice of shape function and smoothness of the exact solution.

Eqn. 1 identifies the convergence problem transferred into the approximation problem. Using first-order linear shape functions, the rate of convergence is of the order $O(h^2)$. Deriving the field quantities from the potential formulation numerically results in a rate of convergence $O(h)$ for these quantities, i.e. a loss in accuracy of one order compared to the potential solution. Using these field quantities, this inherent inaccuracy influences the results of force calculations. This fact identifies the difficulty in obtaining accurate field quantities as a problem of the order of convergence of the numerical method used.

By using an adaptively h-refined FEM discretisation, the size of h varies from element to element. In this case, the order of convergence can be expressed by the degree of freedom (DOF) of the finite element mesh, i.e. for the first order shape functions $O(h^2) = O(DOF^{-1})$.

To surmount the loss in accuracy in a fundamental way, shape functions of higher orders can be used. On the other hand, this would result in fast increasing computational expenses. A good trade-off between both considerations is the use of simple and fast linear shape functions and a local, accurate solution obtained by an analytical formulation, a potential interpolating function yielding derived field quantities of the same order of accuracy as the potential solution. When analysing electromagnetic devices, often local values of the field quantities and the forces are of interest, and therefore the proposed local solutions do not restrict the applicability of the analysis.

For the local two-dimensional field problem, the basic idea is to determine the potential inside a circle

IEE Proceedings online no. 19981469

Paper received 16th January 1997

The authors are with Katholieke Universiteit Leuven, Department of Electrical Engineering, Division ESAT ELEN, Kardinaal Mercierlaan 94, B-3000 Leuven, Belgium

analytically for given potentials applied as the boundary values at its circumference [2, 3]. For three-dimensional field solutions, the local field is determined inside a spherical volume. The boundary values are supposed to be known from previous computations. In both field approaches, a Fourier series is used as the potential formulation to obtain an analytical representation of the derivatives inside the circle, or the sphere. This avoids the loss in order of convergence and accuracy. Although other techniques could be used, the FEM is employed in the preliminary calculation. The boundary values of the local field problem are equally distributed along the circumference of the circle or on the surface of the sphere. From these data the field values in the centre of the circle or the sphere are computed analytically.

Starting from an existing FEM potential solution, the proposed method describes a post-processor operator applied to the air-gap region of an electromagnetic device. No restrictions concerning the finite-element discretisation are assumed. The proposed method is independent of the finite-element mesh inside the domain. The results converge towards the values obtained by the classical evaluation of the potential solution, using numerical derivatives, if a very rough discretisation or unsuitable parameters are chosen, e.g. the number of boundary potential values or the radius of the local field problem. The dependence of the accuracy of the enhanced field solution on the necessary parameters to define the local field problem is discussed, and the suitability of the proposed method is demonstrated by test examples in two and three dimensions.

2 Local field solution

For a more accurate force calculation, the aim is to improve the results of an existing field solution by a local post-process. The idea is to solve the Laplace equation for the magnetic scalar/vector potential $\mathbf{A}$

$$\nabla^2 \mathbf{A} = \frac{\partial^2 A}{\partial x^2} + \frac{\partial^2 A}{\partial y^2} + \frac{\partial^2 A}{\partial z^2} = 0 \qquad (2)$$

in source free and homogenous areas, i.e. in the air gap of an electromagnetic device, starting from an existing potential solution $\mathbf{A}$. The local field problem is defined by the known potential values equally distributed along the circumference of the circle in 2-D or on the surface of a sphere in 3-D, taken as the boundary potential values of the local field problem (Fig. 1). The potential values are calculated at the centre-point P_1 of the circle or the sphere.

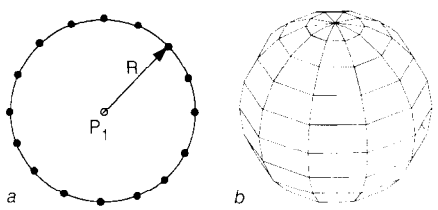

Fig. 1 *Definition of the area of the local field*
a Two-dimensional problems
b Three-dimensional problems

2.1 General two-dimensional approach

The Laplace equation (eqn. 2) written in polar co-ordinates (r, Φ) is

$$\frac{\partial}{\partial r}\left(\frac{r\partial A}{\partial r}\right) + \frac{1}{r}\frac{\partial^2 A}{\partial \Phi^2} = 0$$

$$r^2\frac{\partial^2 A}{\partial r^2} + r\frac{\partial A}{\partial r} + \frac{\partial^2 A}{\partial \Phi^2} = 0 \qquad (3)$$

The idea is to find a function representing formally an infinite series, in which each term is a solution of the partial differential equation, satisfying the boundary values. Assuming linearity and uniformity of the Laplace equation and thus applying it to eqn. 3 a Fourier approach, given in [3, 4], leads to the harmonic function

$$A(r, \Phi) = \frac{\alpha_0}{2} + \sum_{n=1}^{\infty} r^n \{\alpha_n \cos(n\Phi) + \beta_n \sin(n\Phi)\} \qquad (4)$$

with coefficients

$$\alpha_n = \frac{1}{\pi R^n}\int_0^{2\pi} A(R, \Phi)\cdot\cos(n\Phi)d\Phi$$

$$\beta_n = \frac{1}{\pi R^n}\int_0^{2\pi} A(R, \Phi)\cdot\sin(n\Phi)d\Phi \qquad (5)$$

The procedure to solve eqn. 4 describes the solution of a Dirichlet problem on a circle with given boundary values at its circumference. Eqn. 5 represents a Fourier series and the coefficients α_n and β_n can be calculated using the known potentials $A = A(R, \Phi)$ at the circumference of a circle with radius R.

Now a finite number of N equi-angular points is put on the circumference of the circle.

$$A_i(R, \Phi_i) = A\left(R, i\cdot\frac{2\pi}{N}\right) \quad i = 1(1)N \qquad (6)$$

With the N boundary potential values A_i known on the circumference, according to the properties of harmonic functions the first term in eqn. 4 can be written as

$$A|_{r=0} = \frac{\alpha_0}{2} = \frac{1}{N}\sum_{i=1}^{N} A_i \qquad (7)$$

The Fourier coefficients are rewritten as

$$\alpha_n = \frac{2}{N\cdot R^n}\sum_{i=1}^{N} A_i\cos(n\Phi_i)$$

$$\beta_n = \frac{2}{N\cdot R^n}\sum_{i=1}^{N} A_i\sin(n\Phi_i) \qquad (8)$$

With the Fourier series eqn. 4 and its coefficients eqns. 7 and 8, the potential at the centre P_1 of a circle may be computed knowing only the boundary potentials.

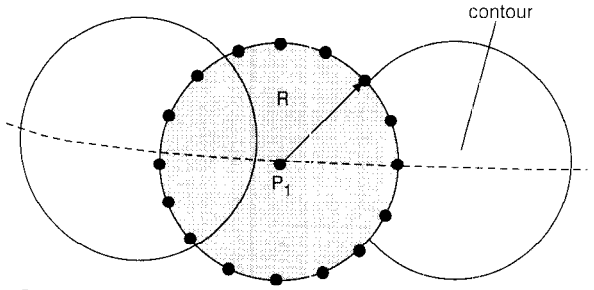

Fig. 2 *Multiple circles determine the potentials at a contour*

Applying eqn. 4, derivatives at the centre of the circle can be calculated. To obtain the potential at a given contour inside a finite element domain, multiple circles

have to be evaluated. Overlapping circles guarantee a continuous solution in the considered region after this post-processor operation (Fig. 2).

The numerical shape of eqns. 4, 7 and 8 enables an easy implementation of the procedure in a finite-element program package. Advantageous is the shape of eqn. 4. The derivatives at the centre of the circle are represented by the Fourier coefficients. Therefore no additional computational effort is required to compute the derivatives at P_1.

$$\left.\frac{\partial A}{\partial x}\right|_{r=0} = a_1 = \frac{2}{N \cdot R}\sum_{i=1}^{N} A_i \cos\Phi_i$$

$$\left.\frac{\partial A}{\partial y}\right|_{r=0} = b_1 = \frac{2}{N \cdot R}\sum_{i=1}^{N} A_i \sin\Phi_i \qquad (9)$$

In order to compare the results obtained by the local field evaluation with conventionally obtained field quantities from first-order elements, Fig. 3, 4 and 5 show the computed vector potential **A** and the derived magnetic flux density in direction x of the Cartesian co-ordinate system with, and without, using the Laplace approach. For the application of the local Dirichlet problem, 24 potential boundary values at the circumference of the circle are used.

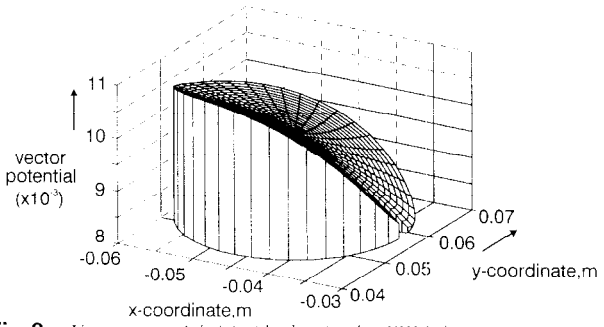

Fig. 3 *Vector potential A inside the circular FEM domain*

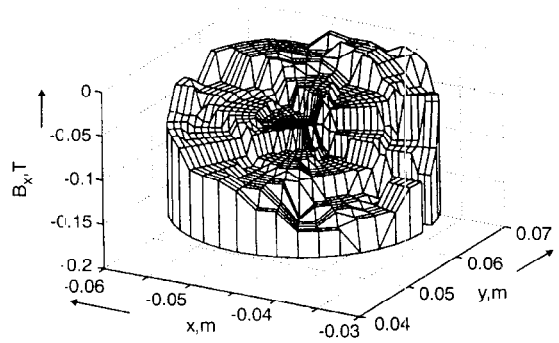

Fig. 4 *Magnetic-flux density B_x by derivation of A*

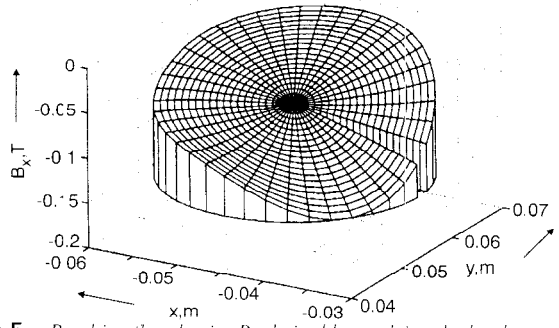

Fig. 5 *Resulting flux density B_x derived by applying the local post-process*

Fig. 3 shows the local vector potential of the FEM solution inside the circular domain. The resulting magnetic flux density using the classical approach $\mathbf{B} = curl\mathbf{A}$ is plotted in Fig. 4. For the finite element discretisation first-order elements were used. It is obvious that forces computed using this type of solution are not reliable. In Fig. 5 the local values of the flux density distribution obtained by solving the described Dirichlet problem, are plotted. It can be seen that this solution is continuous and of the same accuracy when compared to the solution of the vector potential itself (Fig. 3).

2.2 Second approach for cylindrical geometries

A second method uses the values of the magnetic vector potential on two concentric circles with radii R_i and R_o as boundary conditions (Fig. 6). Local field values on the circular contour C with radius $R_i < r < R_o$ are calculated.

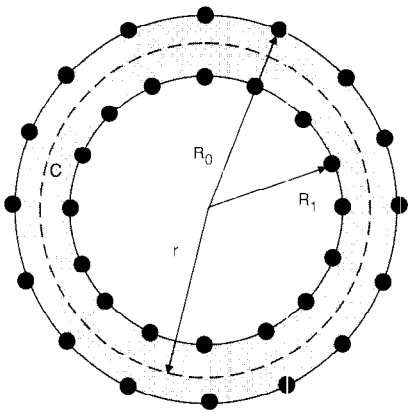

Fig. 6 *Local Dirichlet problem for a cylindrical air gap*

If the inner radius R_i is taken as a reference, the general solution of Laplace's equation is

$$A(r,\Phi) = \sum_{k=1}^{N}\left(a_k\left(\frac{r}{R_i}\right)^k \cos(k\Phi) + b_k\left(\frac{r}{R_i}\right)^k \sin(k\Phi) + c_k\left(\frac{R_i}{r}\right)^k \cos(k\Phi) + d_k\left(\frac{R_i}{r}\right)^k \sin(k\Phi)\right) \qquad (10)$$

The coefficients a_k, b_k, c_k and d_k are independently determined for each circular harmonic. A fast Fourier transformation (FFT) algorithm is used to express the magnetic vector potential at the boundaries as a series of such circular harmonics

$$A(R_i,\Phi) = \sum_{k=1}^{N}(a_{k,i}\cos(k\Phi) + b_{k,i}\sin(k\Phi)) \qquad (11a)$$

$$A(R_o,\Phi) = \sum_{k=1}^{N}(a_{k,o}\cos(k\Phi) + b_{k,o}\sin(k\Phi)) \qquad (11b)$$

$$\begin{bmatrix} 1 & 1 \\ \left(\frac{R_o}{R_i}\right)^k & \left(\frac{R_i}{R_o}\right)^k \end{bmatrix}\begin{bmatrix} a_k \\ c_k \end{bmatrix} = \begin{bmatrix} a_{k,i} \\ a_{k,o} \end{bmatrix} \qquad (12a)$$

$$\begin{bmatrix} 1 & 1 \\ \left(\frac{R_o}{R_i}\right)^k & \left(\frac{R_i}{R_o}\right)^k \end{bmatrix}\begin{bmatrix} b_k \\ d_k \end{bmatrix} = \begin{bmatrix} b_{k,i} \\ b_{k,o} \end{bmatrix} \qquad (12b)$$

Once the magnetic vector potential at the contour C is known, the normal and tangential component of the magnetic flux density can be determined:

$$B_r(r,\Phi) = \sum_{k=1}^{N}\left(-ka_k\frac{r^{k-1}}{R_i^k}\sin(k\Phi)+kb_k\frac{r^{k-1}}{R_i^k}\cos(k\Phi) - kc_k\frac{R_i^k}{r^{k+1}}\sin(k\Phi)+kd_k\frac{R_i^k}{r^{k-1}}\cos(k\Phi)\right) \quad (13a)$$

$$B_t(r,\Phi) = \sum_{k=1}^{N}\left(-ka_k\frac{r^{k-1}}{R_i^k}\cos(k\Phi)-kb_k\frac{r^{k-1}}{R_i^k}\sin(k\Phi) +kc_k\frac{R_i^k}{r^{k+1}}\cos(k\Phi)+kd_k\frac{R_i^k}{r^{k+1}}\sin(k\Phi)\right) \quad (13b)$$

The tangential force component F_t results in the torque T of the device. It can be shown [4, 5] that the value of the torque is given by

$$T = \frac{2\pi}{\mu_0}\sum_{k=1}^{N}(k^2(b_kc_k - a_kd_k)) \quad (14)$$

being independent of the radius r of the contour C. It is not necessary to calculate the normal and tangential component of the magnetic flux density on the contour resulting in a faster algorithm, when the overall torque is aimed at. The proposed method can easily be extended to time-harmonic problems. If all values are rms-values the torque is obtained by adding the torque calculated using the real- and the imaginary-component of the solution.

$$T = T_{real} + T_{imag} \quad (15)$$

2.3 Three-dimensional approach

The local field problem is now defined by the known potential values equally distributed along the surface of a sphere assumed to be the boundary potential values of the local field problem (Fig. 1*b*). According to the co-ordinate transformation

$$x = r\sin\theta\cos\phi$$
$$y = r\sin\theta\sin\phi$$
$$z = r\cos\theta \quad (16)$$

and a spherical co-ordinate system is applied (Fig. 7).

Using the Laplace eqn. 2 with the transformation eqn. 16 yields

$$\frac{1}{r^2}\left[\frac{\partial}{\partial r}\left(r^2\frac{\partial A}{\partial r}\right)+\frac{1}{\sin\theta}\frac{\partial}{\partial\theta}\left(\sin\theta\frac{\partial A}{\partial\theta}\right)+\frac{1}{\sin^2\theta}\frac{\partial^2 A}{\partial\phi^2}\right] = 0 \quad (17)$$

Applying the theorem of the separation of the variables $A(r, \theta, \phi) = R(r) \cdot \Theta(\theta) \cdot \Phi(\phi)$ to eqn. 17, a general form of the functions $R(r)$, $\Theta(\theta)$ and $\Phi(\phi)$ depending on the potential A can be written. Every solution of the Laplace eqn. 17, being finite for all θ, is a solution of

$$A_{m,n}(r,\theta,\phi) = (ar^n + br^{-(n+1)})P_n^m(\cos\theta)\cdot(\alpha\cos m\phi + \beta\sin m\phi) \quad (18)$$

where $m = 0(1)\infty$, $n = m(1)\infty$, a, b, α and β are constants and P_n^m is the associated Legendre polynomial of the first kind. To simplify the notations, the surface harmonics

$$c_{m,n} = P_n^m(\cos\theta)\cdot\cos m\phi$$
$$s_{m,n} = P_n^m(\cos\theta)\cdot\sin m\phi \quad (19)$$

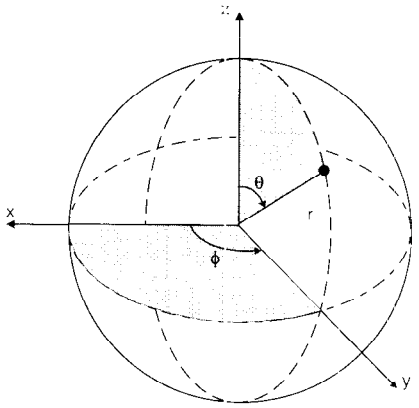

Fig. 7 *Spherical co-ordinate system*

are introduced. Assuming eqn. 18 to be a linear form, the potential in the origin is finite. The constants $\alpha_{m,n}(r)$ and $\beta_{m,n}(r)$ are linear combinations of r^n and $r^{(n-1)}$. The summation

$$A = f(\theta,\phi) = \sum_{m=0}^{\infty}\sum_{n=m}^{\infty}[p_{m,n}\cdot c_{m,n}(\theta,\phi)+q_{m,n}\cdot s_{m,n}(\theta,\phi)]\cdot r^n \quad (20)$$

is a solution of eqn. 17. Here, the magnetic scalar potential A is completely determined by the constants $p_{m,n}$ and $q_{m,n}$. The aim is to calculate the magnetic flux density at a point using known scalar potential values in its vicinity. Consequently, a spherical volume with known boundary potentials at its surface around this field point is chosen to determine the field. The known boundary potentials result from a previously performed FEM computation and determine all constants in eqn. 20. To calculate the magnetic field quantities at the centre of the spherical volume, the Laplace equation has to be solved locally and spherically around this field point with radius $r = R$. The boundary potential values are available only as single values at the surface of the sphere. To distribute them equally along this surface, the spherical co-ordinates ϕ are divided into J and θ giving K equal angles $\Delta\phi$ and $\Delta\theta$, respectively.

$$2\pi = \sum_{j=1}^{J}\Delta\phi$$
$$\pi = \sum_{k=1}^{K}\Delta\theta \quad (21)$$

In order to satisfy eqn. 20 accurately, the number of J and K must be sufficiently large. On the other hand, large numbers rapidly increase the computational expenses. With respect to the computation time and accuracy a good compromise has to be found. Practical values for J and K are given in the following Section.

Assuming ϕ and θ are the co-ordinates in the local system with the interesting field point at the centre of the sphere, the coefficients $P_{m,n}$ and $q_{m,n}$ can be determined by a Legendre decomposition using the

boundary potential values:

$$p_{m,n}|_{m=0} = \frac{\pi}{J \cdot K} \frac{1}{2R^n} \frac{(2n+1)(n-m)!}{(n+m)!} \cdot \sum_{k=1}^{K} \left[\sum_{j=1}^{J} f(\theta_k, o_j) \right] \cdot P_n^m(\cos\theta_k) \cdot \sin\theta_k$$

$$p_{m,n}|_{m>0} = \frac{\pi}{J \cdot K} \frac{1}{R^n} \frac{(2n+1)(n-m)!}{(n+m)!} \cdot \sum_{k=1}^{K} \left[\sum_{j=1}^{J} f(\theta_k, o_j) \cos m o_j \right] \cdot P_n^m(\cos\theta_k) \cdot \sin\theta_k$$

$$q_{m,n} = \frac{\pi}{J \cdot K} \frac{1}{R^n} \frac{(2n+1)(n-m)!}{(n+m)!} \cdot \sum_{k=1}^{K} \left[\sum_{j=1}^{J} f(\theta_k, o_j) \sin m o_j \right] \cdot P_n^m(\cos\theta_k) \cdot \sin\theta_k \quad (22)$$

Retaining the local co-ordinate system in (x', y', z'), the magnetic flux density in the original global co-ordinate system is

$$\mathbf{B} = \mu_0 \mathbf{H} = -\mu_0 \text{grad} \mathbf{A} \quad (23a)$$

or

$$(B_x, B_y, B_z) = -\mu_0 \left(\frac{\partial A}{\partial x'}, \frac{\partial A}{\partial y'}, \frac{\partial A}{\partial z'} \right) \quad (23b)$$

Calculating the derivatives at the origin of the local co-ordinate system (Fig. 7), using $\theta = \pi/2$ and $\phi = 0$ in eqn. 20, yields

$$-\mu_0 \left. \frac{\partial A}{\partial x'} \right|_{(0,0,0)} = -\mu_0 \left. \frac{\partial A}{\partial r} \right|_{(0,0,0)} \quad (24)$$

Analogous to eqn. 24, the derivatives in y are found by taking $\theta = \phi = \pi/2$ and in z by taking $\theta = 0$ and $\phi = \pi/2$, in eqn. 20. With respect to eqn. 24, applying eqn. 23b to eqn. 20 by using eqn. 22 and with the Legendre terms

$$P_1^0(\cos\theta) = \cos\theta$$
$$P_1^1(\cos\theta) = \sin\theta \quad (25)$$

the components of the flux density at the centre of a sphere are explicitly rewritten as

$$B_x = -\mu_0 \frac{3}{2} \frac{\pi}{J \cdot K \cdot R} \cdot \left[\sum_{k=1}^{K} \left(\sum_{j=1}^{J} f(\theta_k, o_j) \cos o_j \right) \cdot \sin^2 \theta_k \right]$$

$$B_y = -\mu_0 \frac{3}{2} \frac{\pi}{J \cdot K \cdot R} \cdot \left[\sum_{k=1}^{K} \left(\sum_{j=1}^{J} f(\theta_k, o_j) \sin o_j \right) \cdot \sin^2 \theta_k \right]$$

$$B_z = -\mu_0 \frac{3}{2} \frac{\pi}{J \cdot K \cdot R} \cdot \left[\sum_{k=1}^{K} \left(\sum_{j=1}^{J} f(\theta_k, o_j) \right) \cdot \cos\theta_k \cdot \sin\theta_k \right] \quad (26)$$

Using this local field approach eqn. 26, by arranging multiple overlapping spheres at an arbitrary surface or contour (Fig. 8), it is possible to obtain the required local field quantities at this surface with the same accuracy as before by FEM-computed potential values. The tetrahedron shown in Fig. 8 represents a part of the three-dimensional mesh of the FEM domain.

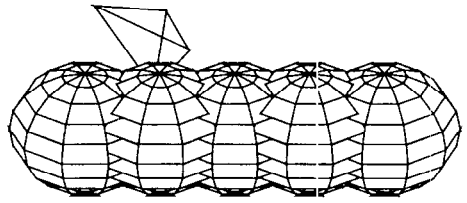

Fig. 8 *Arrangement of multiple overlapping spheres to obtain the local field values on an arbitrary contour across the centre points of the spheres inside a three-dimensional FEM domain*

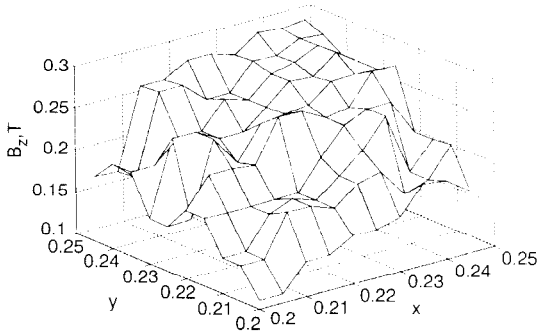

Fig. 9 *Flux density distribution B_z on the front surface of Γ (see Fig. 11) computed by the classical direct derivation of the potential*

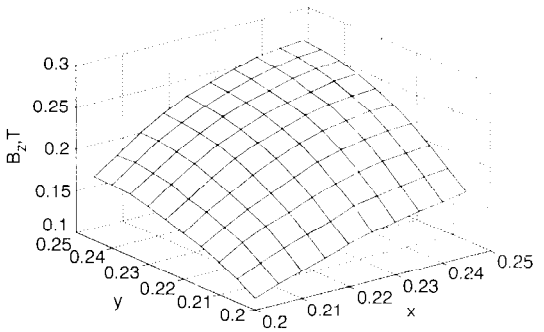

Fig. 10 *Flux density distribution B_z on the front surface of Γ (see Fig. 11) computed using the new proposed post-processor method*

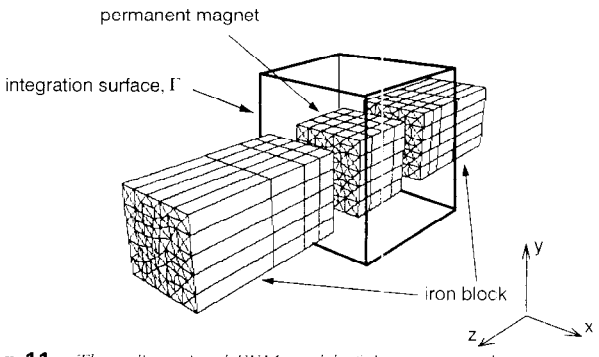

Fig. 11 *Three-dimensional FEM model of the test example*

From Figs. 9 and 10 the difference between the direct evaluation of the potential and the new post-process operator is shown. Here B_z is computed for a test example (Fig. 11) at the front surface of Γ facing the permanent magnet cube. It is obvious that linear shape functions, approximating the scalar potential, are

resulting in a piecewise constant flux density distribution (Fig. 9). Computed forces starting from this type of solution are unreliable. The local values of B_z plotted in Fig. 10 show the expected continuous distribution computed using the new post-processor method.

3 Test examples

3.1 Two-dimensional problems

First method: The method introduced is applied to a magnetostatic field problem. Computations are performed using a test example consisting of a diametrically magnetised circular permanent magnet and a ferromagnetic back iron yoke (Fig. 12). With very dense mesh (Fig. 12*a*) and using eqn. 2 an accurate flux density distribution can be expected. Owing to symmetry, the global force has to be zero. In Fig. 12*b* the computed flux-density distribution is plotted. Owing to the magnetisation direction of the permanent magnet, an angularly sinusoidal normal component of the flux density distribution inside the air gap is expected. Using the local solution, computations are performed on a median circular contour in the air gap. The radius of the individual local circles is taken to be half the air-gap length. Owing to the high discretisation of the finite element domain (Fig. 12*a*) a good agreement between the results obtained by the direct derivation eqns. 2 and 4 is found [4].

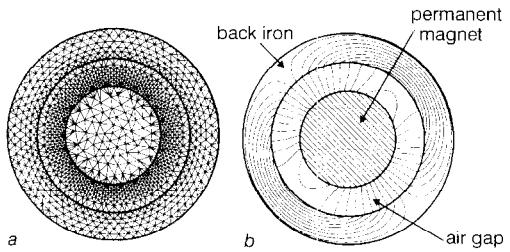

Fig. 12 *FEM discretisation flux plot of the 2-D test example*
a FEM discretisation
b Flux plot

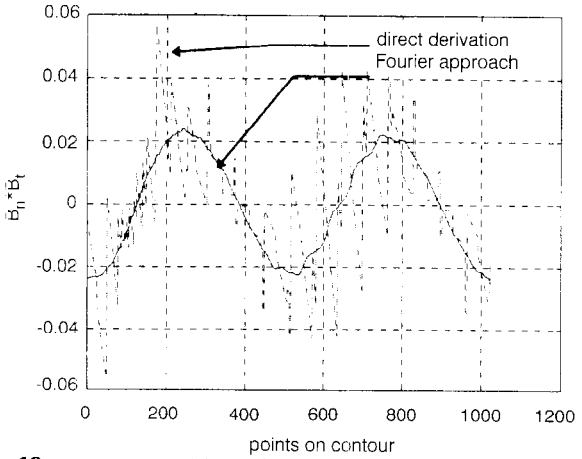

Fig. 13 *Comparison of the product $B_n \cdot B_t$ versus angular position, computed at the median contour in the air gap using both methods*

To compute the force by integrating the Maxwell stress tensor along the median contour in the air gap, the product of normal- and tangential-components of the flux density is necessary. Applying both approaches, the product $B_n \cdot B_t$ is calculated (Fig. 13).

The values obtained by the conventional post-processor show large deviations around the values computed by the local post-processor approach. To obtain accurate results by applying the local post-processor approach, the radius of the circles must be as large as possible and larger than the mesh size. This ensures an increased accuracy of the results compared to the conventional post-processor. Using a less dense finite-element mesh for the local post-processor approach converges towards the same solution-accuracy as obtained by the conventional post-processor method.

Second method: A typical example of a rotating machine with a small air gap is a squirrel cage induction machine. To deal with the non-linearity of the iron and the induced currents in the rotor, a non-linear time-harmonic solution is required [6]. Fig. 14 shows the finite-element model of one quarter of a 4-pole induction machine with 36 stator slots and 28 rotor bars. The air gap consists of 3 layers of elements.

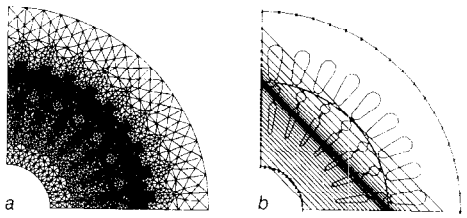

Fig. 14 *Finite element model and outline and constraint plot of the induction machine*

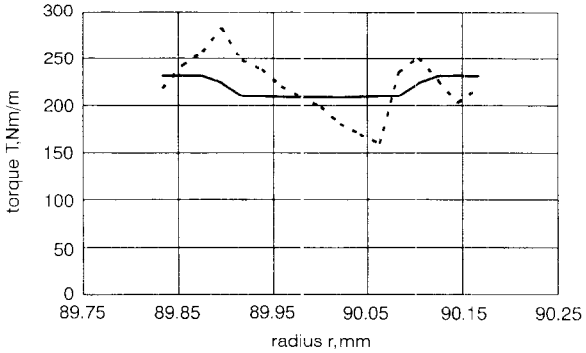

Fig. 15 *Torque variation for different values of the radius r of circular contours C*

Fig. 15 shows the variation of the torque for a varying radius r of a circular contour in the air gap of the induction machine. 1024 points are equidistantly distributed along the contour. The dashed line is the result applying the Maxwell stress method classically. The first contour is placed in the middle of the first layer of elements in the air gap, the last one in the middle of the third layer. The solid line is the result of the Laplace based torque calculation. The result is symmetrical because two contours are needed to calculate the value of the resulting torque of the machine. Fig. 15 shows that the conventional Maxwell stress method strongly depends on the place of the contour inside the air gap, while the Laplace-based method gives similar values for the torque as long as both contours are placed in the middle layer of elements. Furthermore, it is found that the conventional Maxwell stress method is sensitive to the uniformity of the finite elements in the air gap. Uniformity results in a symmetrical torque/radius characteristic.

Measurements on a 400V/50Hz induction machine show very good agreement with the computed data [6].

3.2 Three-dimensional problems

To demonstrate the suitability and accuracy of the proposed method into computing local field values and forces, an example including non-linear soft magnetic

and permanent magnet material is chosen. The test arrangement is symmetrical to its force axis, so a zero resulting force is the theoretically correct solution. The configuration consists of a cubic permanent magnet in the central position between two ferromagnetic blocks. Fig. 11 shows the test arrangement, including the integration surface Γ, used to compute the overall force pulling the permanent magnet cube towards the iron blocks. The magnet is magnetised in the z-direction. The choice of the sphere parameters and the number of boundary potential values at the surface of the arbitrary sphere J and K, are obtained by test calculations. Forces are computed using the Maxwell stress tensor.

In Fig. 16 the force F_z pulling the permanent magnet to one of the iron blocks is plotted. The force is computed only at the front surface of Γ (Fig. 11). Therefore the resulting force is not zero. Applying different numbers of $J = K$ shows that F converges in a stable way towards the accurate value.

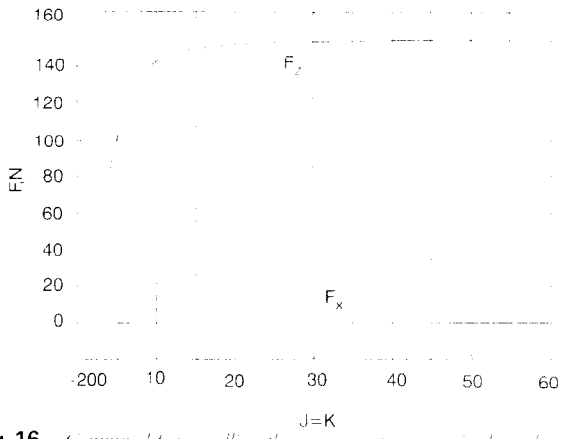

Fig. 16 *Computed force pulling the permanent magnet in the z-direction versus the number of boundary potential values*

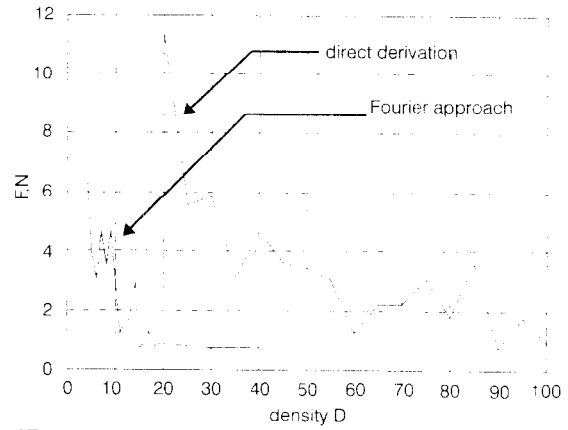

Fig. 17 *Overall force pulling the permanent magnet versus the density D of the boundary values at the surface Γ*

As well as the question of fixing suitable numbers for J and K, a second one rises: how many spheres, i.e. arbitrary field points inside Γ, are required to obtain the complete information out of the potential solution representing the accurate overall field distribution for the force computations? For this purpose the density D is defined. Each side of the cubic surface Γ is now subdivided into an array of D times D equidistant points. In this example, the sphere diameters are set to 0.02m (2% of the characteristic length of Γ). Using the field values at the points, the Maxwell stress tensor is applied to obtain the overall force of the test example. Fig. 17 indicates that a density of $D = 20$ is sufficient to represent the total force accurately. When compared to the force pulling at each side of the magnet cube (Fig. 16), the remaining inaccuracy is less than 0.7% referred to the maximum force. Using the classical direct derivation of the potentials to compute the forces, a far higher density is necessary to obtain the same information. In addition, using the new proposed post-processor operator, the force converges towards a stable value (Fig. 17). Owing to the piecewise constant flux density distribution, the values of the total force computed by the classical approach oscillate and do not converge towards a stable and reliable solution (Fig. 17). Studies regarding the computational efforts required to obtain the full field information from the potential solution show that with $D^2_{derivation} < D^2_{flux} = J \cdot K$, the computation time of the classical method is slightly less compared to the new approach. Nevertheless, the advantage of the new post-process operator supplying the user with a stable and reliable solution makes this method preferable to the classical one, even if the computational costs are higher.

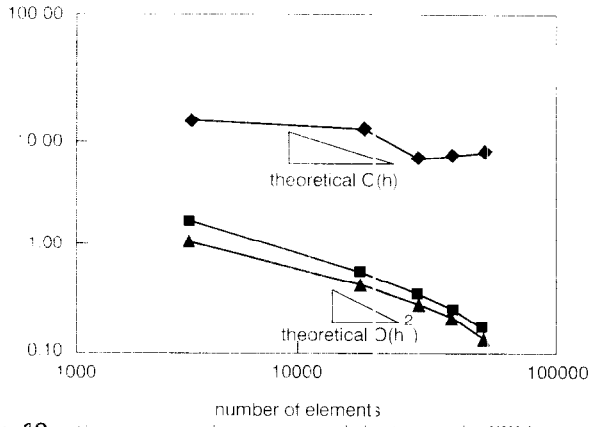

Fig. 18 *Comparison of the convergence behaviour of the FEM potential solution with both the direct derivation and the new proposed method*
- ◆ total force (direct derivation)
- ■ total force (new Fourier approach)
- ▲ total force (FEM potential derivation)

In Fig. 18 the quadratic convergence, referred to the characteristic length h of a finite element, of the FEM potential solution, and the rate of convergence of the force computations using both the classical and the new post-processing approach, is plotted versus the number of tetrahedron elements. The triangles indicate the theoretical gradient of convergence (eqn. 1). The refinement of the three-dimensional discretisation is performed in such a way that the elements are of the same shape in every FEM model in order to obtain a regularly distributed mesh for all cases. To compute the total force, the Maxwell stress tensor is used, integrating the force density calculated in points equidistantly distributed by the density D on all six sides of Γ. For the classical approach, a density $D = 40$ is chosen, and in the case of the new method, D is set to 7. The sphere parameters are $J = K = 15$. The integration surface of the force computations is located in such a way that no plane of Γ cuts through the nodes of the FEM mesh. If nodes are coinciding with the points of the force computation using the classical post-processor approach, this would result in a larger error owing to the troublesome definition of normal and tangential field components in a node of an element. The gradient triangles in Fig. 18 indicate the theoretical rate of convergence for the quadratic and the linear convergence case. It can be seen, as theoretically expected, that the relative error in

an energy norm of the FEM potential solution converges quadratically, referred to the specific diameter h of the elements (see eqn. 1), by increasing the number of first-order tetrahedron elements. Owing to the analytically described potential function inside the local field volumes, the resulting overall force using this approach is of the same order of convergence. Therefore no loss of accuracy of the derived field quantities occurs. The convergence of the total forces, computed by the classical approach, indicates the expected linear behaviour. The accuracy of the computed values is influenced by the numerically obtained derivatives. This shows that the results obtained by the classical method are inherently inaccurate when compared to the accuracy of the potential solution.

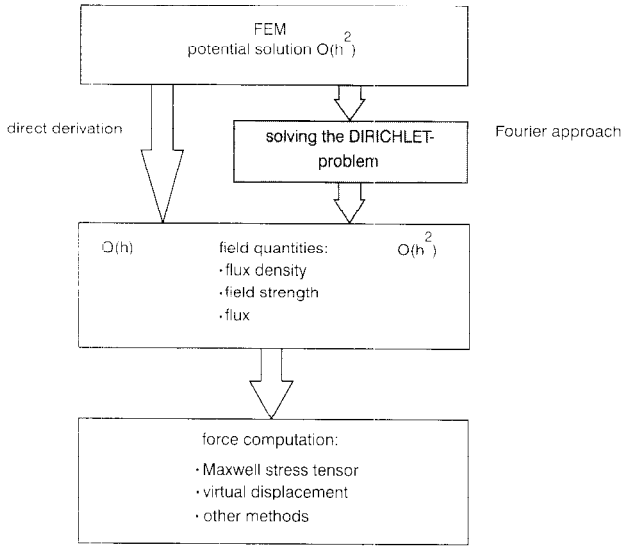

Fig. 19 *Additional step during post-processing to enhance the accuracy of derived field quantities*

4 Implementation

The use of the new proposed methods to enhance the accuracy of computed field quantities, starting from an existing potential solution, demands an additional step during the post-processing of the FEM analysis (Fig. 19). Having obtained an FEM potential solution, the user only has to define the surface of integration Γ on which the field quantities or forces have to be calculated. This is performed by defining single planes in the air gap of the three-dimensional FEM model. Defining an arbitrary contour allows the computation of field quantities or forces along it as well. For each plane or contour, the density D, the sphere parameter J, K and the radius R have to be set. The sphere parameters are problem dependant and related to the geometry of the device, i.e. the air-gap width. The planes or contours should be centred in the air gap. A suitable value for the diameter of the single spheres is about 90-95% of the air-gap width in order to have as many tetrahedron finite elements inside the sphere as possible. Including only one finite element in the sphere results in no enhancement in accuracy of the derived quantity. To ensure a continuous field solution, the density D should be chosen in such a way that the spheres overlap (Fig. 8). For the distance between two points on the surface of integration, it is suitable to choose the radius of the sphere.

To define the number and position of boundary potential values distributed on the surface of each sphere, the parameters J and K have to be chosen. To ensure uniformly distributed boundary values J is set equal to K. In accordance with the results of Fig. 17 and other test calculations, a number $J = K = [10 \ldots 20]$ is sufficient to meet the ratio between computational costs and accuracy. Fig. 20 illustrates by different $J = K$ the position and number of the boundary potentials to approximate the local field inside a sphere.

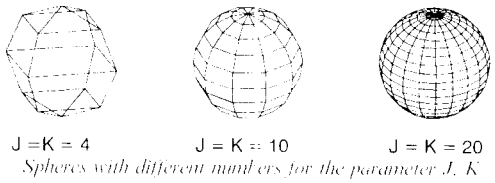

Fig. 20 *Spheres with different numbers for the parameter J, K*

5 Conclusions

The local solution of the Laplace eqn. 2 inside the air gap of an electromagnetic device, using a Fourier series approximation as the potential function, results in a significant increase in accuracy of the derived field quantities. Inherently inaccurate solutions obtained by numerically derived field values are caused by the loss of one order of rate of convergence when the derived quantities are compared to the potential solution. This problem occurs in two- and three-dimensional field problems. A solution for the 2-D and 3-D problems is discussed. The basic idea of solving a Dirichlet problem in a local post-processor is introduced. This method describes a technique to enhance the accuracy of derived field quantities, i.e. field values and forces, derived from a potential solution. Here, a finite element solution applying standard linear 2-D triangles and 3-D tetrahedrons is used. Solving a local Dirichlet problem inside a circle in 2-D or a sphere in 3-D analytically, enhances the accuracy of the derived field quantities of a finite element model. Fourier series are used to represent the potential function of the local field problem. Necessary parameters are introduced and suitable numbers are given. With this approach, it is shown that the rate of convergence for the field solution is the same as that of the FEM potential solution itself. Two- and three-dimensional FEM test examples including permanent magnet material demonstrate the behaviour of the proposed methods. Results for local field values and forces point out their suitability. The comparison of computed forces using the classical post-processor approach and the new post-process operator show the advantage regarding both accuracy and stability of solutions obtained by the proposed method.

In combination with lower-order finite elements, a local solution of Laplace's equation results in more accurate local field values for a given computation time. A higher accuracy for force and torque is obtained using these field values in the Maxwell stress method.

6 Acknowledgments

The authors are indebted to the Belgian 'Nationaal Fonds voor Wetenschappelijk Onderzoek' for its financial support for this work and the Belgian Ministry of Scientific Research for granting the IUAP No. 51 on Magnetic Fields.

7 References

1 ZIENKIEWICZ, O.C., and TAYLOR, R.L.: 'The finite element method' *in* 'Basic formulation and linear problems, vol. 1' (McGraw Hill, 1994, 4th edn.)

2 KASPER, M., and FRANZ, J.: 'Highly accurate computation of field quantities and forces by superconvergence in finite elements', *IEEE Trans. Magn.*, 1995, **31**, (3), pp. 1424–1427

3 MEIS, TH., and MARCOWITZ, U.: 'Numerical solution of partial differential equations', *Appl. Math. Sci.*, 1981, **32**, (Springer Verlag)

4 MERTENS, R., DE WEERDT, R., PAHNER, U., HAMEYER, K., and BELMANS, R.: 'Force calculation based on a local solution of Laplace's equation', Proceedings 7th biennial IEEE conference on *Electromagnetic field computation*, CEFC'96, Okayama, Japan, 19-20 March 1996, pp. 354

5 SALON, S.J.: 'Finite element analysis of electrical machines' (Kluwer Academic, Boston, London, Dordrecht, 1995)

6 DE WEERDT, R., HAMEYER, K., and BELMANS, R.: 'End winding leakage calculation of a squirrel-cage induction motor for different load conditions', *COMPEL – Int. J. Comput. Math. Electr. Electron. Eng.*, 1995, **14**, (4), pp. 85–88